Computer Simulation of the Damage Evolution of Fiber-Reinforced Polypropylene-Matrix Composites with Matrix Defects

Hongzhou Li,[1] Yuxi Jia,[1,2] Geni Mamtimin,[3] Wei Jiang,[1] Lijia An[1]

[1]*State Key Laboratory of Polymer Physics and Chemistry, Changchun Institute of Applied Chemistry, Graduate School of the Chinese Academy of Sciences, Changchun 130022, China*
[2]*School of Materials Science and Engineering, Shandong University, Jinan 250061, China*
[3]*School of Mechanical Engineering, Xinjiang University, Urumqi 830008, China*

Received 17 August 2005; accepted 19 December 2005
DOI 10.1002/app.23965
Published online in Wiley InterScience (www.interscience.wiley.com).

ABSTRACT: The damage evolution of fiber-reinforced polypropylene-matrix composites with matrix defects was studied via a Monte Carlo technique combined with a finite element method. A finite element model was constructed to predict the effects of various matrix defect shapes on the stress distributions. The results indicated that a small matrix defect had almost no effect on fiber stress distributions other than interfacial shear stress distributions. Then, a finite element model with a statistical distribution of the fiber strength was constructed to investigate the influences of the spatial distribution and the volume fraction of matrix defects on composite failure. The results showed that it was accurate to use the shear-lag models and Green's function methods to predict the tensile strength of composites even though the axial stresses in the matrix were neglected. © 2006 Wiley Periodicals, Inc. J Appl Polym Sci 103: 64–71, 2007

Key words: composites; mechanical properties; Monte Carlo simulation

INTRODUCTION

The damage and failure of a unidirectional fiber composite are a complex event. The fiber with the weakest defect breaks first. The load carried by the broken fiber is then transferred to other fibers and even possibly to the matrix as well. Matrix yielding, interfacial debonding, and interfacial sliding around the fiber break can inhibit the crack propagating into the matrix. After the first fiber break occurs, the load carried by the broken fiber is then redistributed among the remaining intact fibers and the matrix as determined by the constitutive response of the fibers, matrix, and interface. Stress redistribution causing stress concentration can induce other fibers to fail according to the statistical distribution of the fiber strength and thus sheds further load to the intact fibers and the matrix. As increasing load is applied to the composite, critical damage cluster comes into being. The greater the number of broken fibers required to create the requisite critical damage cluster is, the more reliable the composite is. Before a global instability that can cause macroscopic failure is initiated, more fibers have to break. When the damage of the fibers and matrix accumulates to some point, the composite as a whole will be unable to carry any additional load, and failure will be inevitable. To handle the complex damage evolution of composites with many fibers, the break influence and Green's function methods have been developed by a number of workers.[1–14]

As the broken fiber propagates its crack into the matrix, the matrix will crack, and the load carried by the cracked matrix will be transferred predominantly onto the nearby fibers. Because composites are sensitive to matrix defects, matrix fracture can induce composite fracture in which fiber and matrix fractures progress unstably from around a single break. However, most existing models for stress transfer have neglected the stress carried by the matrix and the possibility of matrix fracture. To avoid matrix fracture, composites can be manufactured with specific matrices or specific fiber/matrix interfaces. However, it is hard to avoid matrix defects during processing. Therefore, the design and optimization of fiber-reinforced polymer-matrix composites require attention to be paid to the detailed micromechanics of load transfer and damage evolution around individual fiber breaks and matrices with defects.

Correspondence to: Y. Jia (jia_yuxi@sdu.edu.cn) and L. An (ljan@ciac.jl.cn).

Contract grant sponsor: National Natural Science Foundation of China; contract grant numbers: 50373044, 50573079, 50390090, 50403009, and 50340420392.

Contract grant sponsor: Chinese Academy of Sciences; contract grant number: KJCX2-SW-H07.

Contract grant sponsor: Special Funds for National Basic Research Program of China; contract grant number: 2003CB615600.

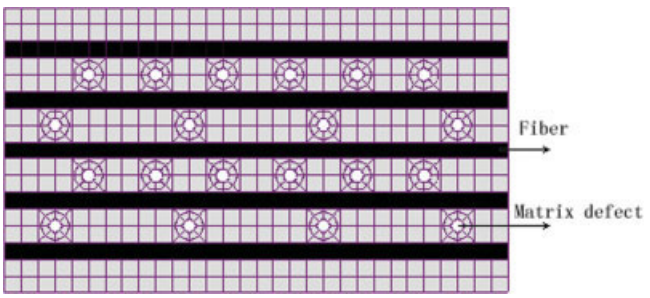

Figure 1 Schematic drawing of the finite element model and the mesh of a multifiber-reinforced polypropylene-matrix composite with matrix defects. [Color figure can be viewed in the online issue, which is available at www.interscience.wiley.com.]

Employing a Monte Carlo technique combined with a finite element method, we simulated the damage evolution of fiber-reinforced polypropylene-matrix composites with matrix defects. In the absence of a detailed knowledge of the underlying mechanics at the micro- and mesoscales,[15] damage and failure were represented with internal damage parameters under the assumption that there exist some distributed damages in composites. First, we studied the effects of the shape and size of a small matrix defect on stress distributions. Then, we investigated the influences of the spatial distribution and the volume fraction of many matrix defects on the composite strength through a combination of a Monte Carlo technique with a finite element method, and we performed a statistical analysis to determine the probability that a fiber with intrinsic flaw distributions would fail.

It has been proved by experiments that interfacial defects are the dominant factors for evaluating the nonlinear behavior and strength of composites.[16,17] However, the interfacial quality can be improved by the coating of reinforcing fibers with a coating layer. The poor low-speed-impact resistance (i.e., low energy absorption before major failure) of stiff-fiber-reinforced composites can be improved by the coating of the reinforcing fibers with a very thin elastomeric coating.[18] A coating layer that can form interfacial oxides at high temperatures increases the interfacial shear stress and prevents the interface from debonding and the crack from propagating into the matrix or the fibers. We will study how the interfacial defects affect the damage evolution of fiber-reinforced polymer-matrix composites in the future.

SIMULATION METHODOLOGY

Finite element model

Because of the very complicated nature of composite materials, finite element modeling is perhaps the best candidate for investigating the damage evolution of fiber-reinforced polymer-matrix composites. Finite element analysis provides useful insight into the behavior of a material at the microscopic level. As an example, we considered the generation of a two-dimensional finite element mesh for studying the damage evolution process of fiber-reinforced polypropylene-matrix composites with matrix defects. Figure 1 shows the finite element model and the mesh, in which eight-node isoparametric quadratic elements based on a plane stress condition were used in the mesh discretizations of matrix and fibers. Fifty fibers were embedded into the finite element mesh with equal interfiber spacing, and the volume fraction of the fibers was 30%. The principle of virtual work was used to determine the stiffness of the fibers and the matrix. The matrix region between any two consecutive fibers was filled with matrix defects. The diameter of the matrix defect was 30, 50, or 70 μm. We assumed that defects with different shapes occurred in the matrix. Figure 2 depicts the square, hexagonal, and circular defects of the matrix in our model. Matrix defects of other geometrical shapes can also be modeled, but including them in the model will bring difficulty to finite element discretization and not increase the accuracy of the solution significantly. Although we used only three types of representative defects for this study, the procedure was general and independent of the shapes of the defects. When we investigated the influence of the spatial distribution and the volume fraction of many matrix defects on composite failure, the spatial distribution of these defects was assumed to obey a hexagonal distribution. The axial length of the model was chosen so that the stress distribution at the boundary of the model was not disturbed by the stress redistribution caused by the introduction of fiber damage. The fiber element length was discretized into a set of finite elements with the length less than the characteristic length (L_c). The stress transfer across the fiber/matrix interface due to interfacial shear sliding was accomplished via contact (gap) elements. Because of the very low yield stress of the matrix and the high strength and stiffness of the fiber, the stress–strain behavior of the composite is nearly linear over the entire range of loading. In the absence of fiber damage, uniaxial loading determines the overall stress–strain response of the undamaged

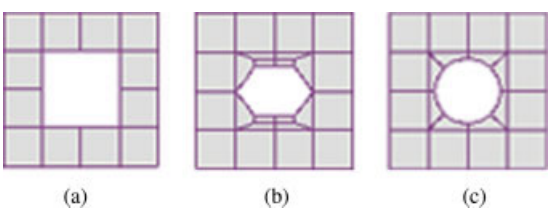

Figure 2 Three different shapes of matrix defects: (a) a square defect, (b) a hexagonal defect, and (c) a circular defect. [Color figure can be viewed in the online issue, which is available at www.interscience.wiley.com.]

composite. Typically, for a large composite, the stress–strain behavior will follow that of an undamaged one up to the failure stress because the effect of localized fiber damage on the overall composite deformation is rather small up to the failure. The Von Mises formulation and the isotropic plastic hardening condition were assumed to describe the plastic behavior of the matrix. The stress–strain relation of the matrix was constructed with the so-called J_2 flow theory:

$$\dot{\sigma} = L_{ijkl} : \dot{\varepsilon} \tag{1}$$

$$L_{ijkl} = l_{ijkl} - \frac{\alpha}{g}\frac{E^2}{(1+\nu)^2}\sigma'_{ij}\sigma'_{kl} \tag{2}$$

$$g = \frac{4}{9}EY^2\left[\frac{E^p}{E} + \frac{3}{2(1+\nu)}\right] \tag{3}$$

$$l_{ijkl} = \frac{E}{1+\nu}\left[\frac{1}{2}(\delta_{ik}\delta_{jl} + \delta_{il}\delta_{jk}) + \frac{\nu}{1-2\nu}\delta_{ij}\delta_{kl}\right] \tag{4}$$

where $\dot{\sigma}$ is the stress increment, $\dot{\varepsilon}$ is the strain increment, σ'_{kl} is the deviatoric stress tensor; L_{ijkl} is the elastoplastic tensor, l_{ijkl} is the elasticity tensor, E is the elastic modulus, ν is the Poisson ratio, E^p is the plastic modulus, σ'_{ij} is the deviatoric stress tensor, Y is the hardness parameter, and δ is the Kronecker delta. When the matrix is an elastic body, α is 0, and when the matrix is an elastic–plastic body, α is 1.

If the equivalent stress of a fiber element reaches its preset tensile strength value based on the Weibull distribution, the Young's modulus of the fiber element is changed to zero. Then, the fiber element is assumed to lose all its static stresses. If the equivalent stress of a matrix element reaches its tensile strength value, E of the matrix element is changed to zero. Then, the matrix element is also assumed to lose all its static stresses. If the interfacial shear stress reaches the interfacial shear strength, it is thought that interfacial debonding occurs.

Statistical strength distribution of the fibers

A fiber has scattering in its strength because of the random distribution and various sizes of flaws or cracks along the fiber surface or in the fiber. The strength of a fiber is always evaluated by the Weibull distribution. Typically, the statistical distribution of the fiber strength is measured directly by the performance of a single-fiber tension test on a set of fibers with a common gauge length (L). It is assumed in this simulation that the strength of each fiber obeys the Weibull distribution.

The two-parameter Weibull distribution function [$F(\sigma,L)$] for a fiber element with some random strength (σ_F) is given as follows:[19–28]

$$F(\sigma, L) = P_F(\sigma \geq \sigma_F) = 1 - \exp\left[-\frac{L}{L_0}\left(\frac{\sigma}{\sigma_0}\right)^{m_F}\right] \tag{5}$$

where σ denotes the stress, P_F is the cumulative probability of failure for each fiber element (its value ranges from 0 to 1, generated by a uniform random number), σ_0 is the Weibull scale parameter describing the strength of a fiber with length L_0 in a tension test, m_F is the Weibull shape parameter (the Weibull modulus) describing the statistical spread in strength, L_0 is the standard gauge length at which the two Weibull parameters are estimated, and L is the fiber element length.

In the finite element simulations, each fiber is discretized into a set of finite elements with length L:[15,19]

$$\sigma_c = \left(\frac{\sigma_0^{m_F}\tau L_0}{r}\right)^{1/1+m_F}; \; L_c = \frac{r\sigma_c}{\tau} = \left(\frac{r\sigma_0 L_0^{1/m_F}}{\tau}\right)^{m_F/m_{F+1}}; \qquad L \ll L_c \tag{6}$$

where σ_c is the characteristic fiber strength in a composite, r is the radius of the fiber, and τ is the interfacial shear stress.

Deduced from formula (5), the random strength of a fiber element (σ_F) is given as follows:

$$\sigma_F = \sigma_0\left[-\frac{L_0}{L}\ln(1 - P_F)\right]^{1/m_F} \tag{7}$$

By the substitution of uniform random numbers in a range of 0–1 into eq. (5), σ_F can be obtained. The uniform random numbers are generated via a pseudorandom number generator. Assigning the obtained Weibull strengths to each fiber element can randomly generate the strength of each fiber element. The lowest strength value generated is always assigned to the centrally located parts of the elements to ensure that the failure takes place away from the specimen ends.

r_{min} method

The computation is carried out under the boundary condition of a displacement increment at the fiber and matrix ends that is related to a uniform applied strain, and the increment width is determined by the r_{min} method, which was developed by Yamada et al.[29] and Goda.[30,31] The stress increment required to break an element can be solved from r_{min}, which is the minimum value of the incremental ratio. In each simulation, the applied displacement is increased step by step with small enough steps that at most one or two elements will fail in each step. At the first calculation step of this simulation, an arbitrary displacement large enough to damage almost all the elements is given to the boundaries. Then, the calculated displacements are changed to the exact displacements by the multiplication of r_{min} to the displacement increment for each ele-

ment. The stresses and loads acting on the elements are calculated from the computed displacements. In the *i*th-stage computation, the stresses of the fiber, matrix, and interfacial element are as follows:[30]
For the fiber

$$(\sigma_f)_i = (\sigma_f)_{i-1} + (\Delta\sigma_f)_i \tag{8}$$

For the matrix

$$(\sigma_x)_i = (\sigma_x)_{i-1} + (\Delta\sigma_x)_i, \quad (\sigma_y)_i = (\sigma_y)_{i-1} + (\Delta\sigma_y)_i, \quad (\tau_{xy})_i = (\tau_{xy})_{i-1} + (\Delta\tau_{xy})_i \tag{9}$$

For the interface

$$(\tau)_i = (\tau)_{i-1} + (\Delta\tau)_i \tag{10}$$

where σ_{i-1} is the determined stress increment of each element at the $i-1$th calculation and $\Delta\sigma_i$ is the arbitrary and tentative stress increment at the ith calculation.

To allow all element stresses to reach their corresponding strengths, the following equations must be satisfied:[30]
For the fiber

$$(\sigma_f)_{i-1} + r(\Delta\sigma_f)_i = \sigma_F \tag{11}$$

For the matrix

$$\{(\sigma_x)_{i-1} + r(\Delta\sigma_x)_i\}^2 - \{(\sigma_x)_{i-1} + r(\Delta\sigma_x)_i\} \times \{(\sigma_y)_{i-1} + r(\Delta\sigma_y)_i\} + \{(\sigma_y)_{i-1} + r(\Delta\sigma_y)_i\}^2 + 3\{(\tau_{xy})_{i-1} + r(\Delta\tau_{xy})_i\} = \sigma_M^2 \tag{12}$$

For the interface

$$(\tau)_{i-1} + r(\Delta\tau)_i = \tau_I \tag{13}$$

where σ_F is the assigned Weibull strength of fibers, σ_M is the matrix strength, τ_1 is the interfacial shear strength, and r is the ratio equalizing the left side with the right side. That is, r is an index that judges the degree of damage, and it is calculated with eqs. (11)–(13) for each element as follows:[30]
For the fiber

$$r = \frac{\sigma_F - (\sigma_f)_{i-1}}{(\Delta\sigma_f)_i} \tag{14}$$

For the matrix

$$r = \frac{-b + \sqrt{b^2 - 4ac}}{2a} \tag{15}$$

where:

$$a = \{(\Delta\sigma_x)_i\}^2 + \{(\Delta\sigma_y)_i\}^2 - (\Delta\sigma_x)_i(\Delta\sigma_y)_i + 3\{(\Delta\tau_{xy})_i\}^2$$

$$b = 2\{(\sigma_x)_{i-1}(\Delta\sigma_x)_i + (\sigma_y)_{i-1}(\Delta\sigma_y)_i\} - \{(\sigma_x)_{i-1}(\Delta\sigma_y)_i + (\sigma_y)_{i-1}(\Delta\sigma_x)_i\} + 6(\tau_{xy})_{i-1}(\Delta\tau_{xy})_i$$

$$c = \{(\sigma_x)_{i-1}\}^2 + \{(\sigma_y)_{i-1}\}^2 - (\sigma_x)_{i-1}(\sigma_y)_{i-1} + 3\{(\tau_{xy})_{i-1}\}^2 - \sigma_M^2$$

For the matrix

$$r = \frac{\tau_I - (\tau)_{i-1}}{(\Delta\tau)_i} \tag{16}$$

Only the element giving the minimum ratio of all the elements suffers the damage, that is, the fiber break, the matrix cracking, or the interfacial debonding. Finally, the exact stresses are given as follows:[30]
For the fiber

$$(\sigma_f)_i = (\sigma_f)_{i-1} + r_{\min}(\Delta\sigma_f)_i \tag{17}$$

For the matrix

$$(\sigma_x)_i = (\sigma_x)_{i-1} + r_{\min}(\Delta\sigma_x)_i, \quad (\sigma_y)_i = (\sigma_y)_{i-1} + r_{\min}(\Delta\sigma_y)_i, \quad (\tau_{xy})_i = (\tau_{xy})_{i-1} + r_{\min}(\Delta\tau_{xy})_i \tag{18}$$

For the interface

$$(\tau)_i = (\tau)_{i-1} + r_{\min}(\Delta\tau)_i \tag{19}$$

By the multiplication of $r_{\min}$ with its increment, the exact strain and displacement can be calculated.

Simulation procedure

The Weibull random numbers with respect to both the strength and critical damage quantity are independently assigned to each fiber element, and the spatial distribution of the matrix defects is assumed to obey a hexagonal distribution.

Under the boundary condition of displacement increment, an arbitrary displacement is given along the fiber axis direction at each fiber end.

Then, in the displacement process, whether a fiber element breaks or not is checked by a comparison of the Weibull strength value of the fiber with its equivalent stress value. If the Weibull strength value of each fiber element is less than its equivalent stress value, and the equivalent stress value of each matrix element is less than its tensile strength value, the displacement increment proceeds. Otherwise, the fiber element or the matrix element is regarded as broken, and the Young's modulus of the fiber element or the matrix element is then changed to zero, and so are the strain–stress components of this element. The stress is redistributed according to the finite element stress analysis, and this element is assumed to lose all its static stresses; that is, the load acting on this element is released through its nodes along the displacement direction under the boundary condition of the load increment.

Finally, as the damage accumulates in the composite, the pseudonodal loads along the fiber axis direction decrease largely at a certain strain. It is assumed that when the average of the fiber element stresses in

TABLE I
Material Constants Used in the Simulation

Material	E (GPa)	ν	σ_b (MPa)	σ_y (MPa)	r (um)	σ_0 (GPa)
Fiber	395	0.33	2500 (1 mm)	142	2.6 (1 mm)	
Polypropylene	1.35	0.36	37.7	32.5		

σ_b, the tensile strength; σ_y, the yield stress.

the composite decreases below 90% of the maximum of the average stress before a given applied strain is achieved, or when there are sufficient failed elements to cause catastrophic damage propagation in one cycle, the composite damage criterion is satisfied. The stress applied just before failure is taken as the strength of the composite.

EXAMPLES

Table I lists the key data used in the simulation. Inputs for the model consist of geometrical and material parameters. Some of the parameters can be obtained from micromechanical measurements or arguments, whereas others are empirical and are determined by the calibration of the model against experimental test data. Comparing the results obtained from the finite element simulation of the deformation of a tensile specimen with the data available from mechanical tests and making suitable modifications can considerably improve the accuracy of the data.

A polypropylene-matrix monolayer composite was used in the simulation. The polypropylene matrix was considered an elastic–plastic matrix.

RESULTS AND DISCUSSION

Stress distribution around a single matrix defect

The precise stress distribution of a fiber-reinforced polypropylene-matrix composite with a small matrix defect (not shown in this article) is complicated by bending and compatibility requirements in the region of the stress concentration. There is an obvious gradient in the axial stress of the nearest neighboring fibers through the cross section near the matrix defect, although the stresses at farther neighbors are more uniform. Figure 3 shows the stress concentration factors of the fiber elements next to a matrix defect element, which are perpendicular to the fiber axis. The diameter of the matrix defect is 50 μm. The average stress concentration factors (averaged over the fiber cross section) of the nearest neighbor fibers for the three shapes of matrix defects are all about 1.005, and they decrease slowly with increasing applied load. Figure 4 shows the normalized axial stress on the nearest neighboring fiber next to the matrix defect as a function of the distance from the matrix defect element. The stress concentration factor decreases a little and falls below unity before recovering to unity at larger distances. The reduction of the stress concentration factor below unity is partially due to bending but primarily due to the necessity of satisfying the compatibility condition. Therefore, there must be a region along each neighboring fiber in which the stress and strain are reduced below the far-field values so that the net additional displacement induced by the defect in the far field is zero. The stress recovery of the matrix is relatively rapid and independent of the shape of the matrix defect. Near the matrix defect, the stresses of the nearest neighboring fibers are larger than those in

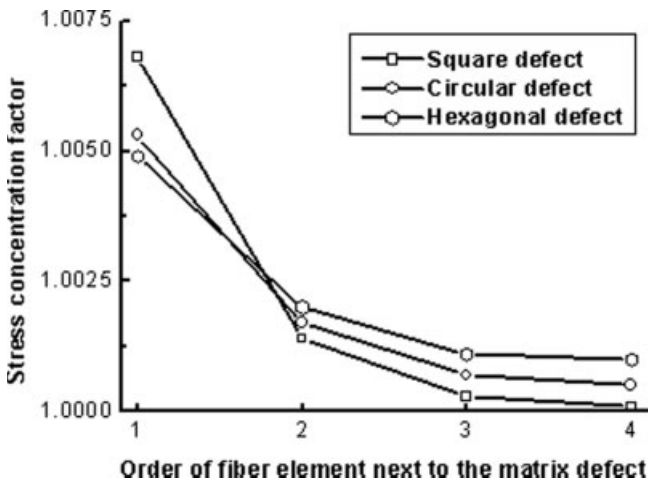

Figure 3 Stress concentration factors of the fiber elements next to a matrix defect element, which are perpendicular to the fiber axis.

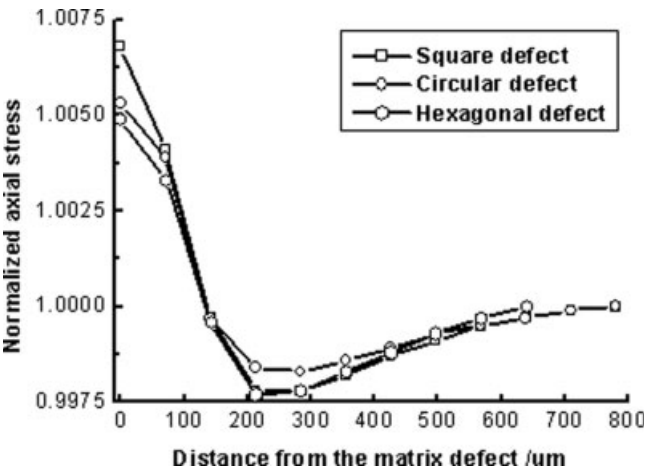

Figure 4 Normalized axial stress on the nearest neighboring fiber next to a matrix defect.

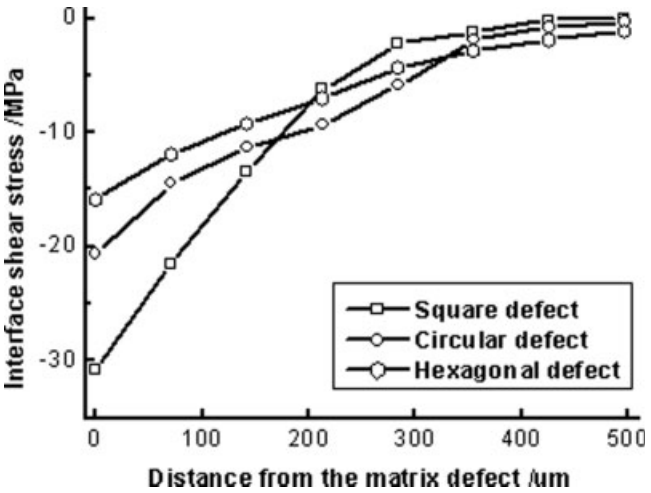

Figure 5 Interfacial shear stress on the nearest neighboring fiber next to a matrix defect.

the far field, inducing additional displacement and strain. However, the strain field is uniform across the fibers far from the defect. Figure 5 shows the interfacial shear stress on the nearest neighboring fiber next to the matrix defect as a function of the distance from the matrix defect element. The introduction of a small matrix defect in the model induces an obvious change in the local shear stress around it. For circular and hexagonal matrix defects, the shear stresses are distributed quite uniformly within a sliding zone just away from the matrix defect and then decay smoothly to zero. For the square matrix defect, the shear stress shows more rapid variation within the sliding region.

For handling the effect of the size of the matrix defect on the stress distribution, we have only considered the circular matrix defect. The diameter of the matrix defect is 30, 50, or 70 μm. Compared with the fiber radius of 142 μm, the matrix defect is relatively small. The contributions of the square matrix defects with different sizes to the stress concentration on the nearest neighboring fibers are almost the same. The tensile load in the fiber-reinforced composite is mainly carried by the stiff fibers, primarily because of the very low matrix/fiber stiffness ratio.

From these simulation results, we conclude that there are almost no influences of the shape and size of a small matrix defect on the stress distribution of fiber-reinforced polypropylene-matrix composites, except for the interfacial shear stress distribution. Therefore, we can neglect the effects of the shape and small size of matrix defects on stress redistributions for the damage evolution simulation of fiber-reinforced polypropylene-matrix composites.

Fiber damage evolution with matrix defects

To predict the strengths of a relatively large composite, hundreds of simulations of failure in composites having several hundred fibers are required. The unit cell models are limited to symmetric clusters of fiber breaks because of the symmetry of the unit cell, and the embedded cell models are limited to the mechanical behavior of composites in the cross direction.[32] The axial stresses in the matrix and the radial axial stress distribution within the fibers are ignored in the shear-lag modes and Green's function methods. It is insufficient to focus fiber damage evolution on a single matrix defect only. Investigating the influence of the spatial distribution of matrix defects on composite failure must incorporate a Monte Carlo technique. It is not computationally feasible to simulate very large samples via the finite element methods to retain the necessary details at the smallest scale around all of the damage sites. Hence, we considered only a relatively small number of fibers in our simulation.

Simulations were performed on a one-ply unidirectional polypropylene-matrix composite with 50 fibers. Figure 6 shows the normalized applied stress versus the strain of polypropylene-matrix composites with and without matrix defects. The y axis represents the applied stress of composites with different matrix defect volume fractions (MDVFs) divided by their own tensile strength. The stress–strain relationship is linear up to $\varepsilon = 1.1\%$ for the composites having various MDVFs. Over the range of $\varepsilon = 1.1$–2.6%, the composite is strain-hardened. After the strain reaches 2.6%, the composites start to fail. The tensile strain is increased when the MDVF in the composite increases. The finite element simulation has predicted the spatial positions and applied stress levels for the fiber breakpoint. Figure 7 shows the applied stress of the composites with and without matrix defects, normalized by their own tensile strength, as a function of the number of fiber breakpoints. As successive fibers break at increasing

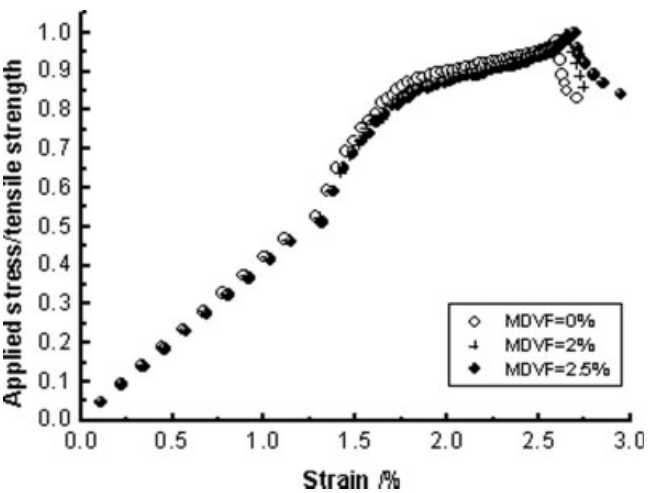

Figure 6 Normalized applied stress versus the strain of polypropylene-matrix composites with and without matrix defects.

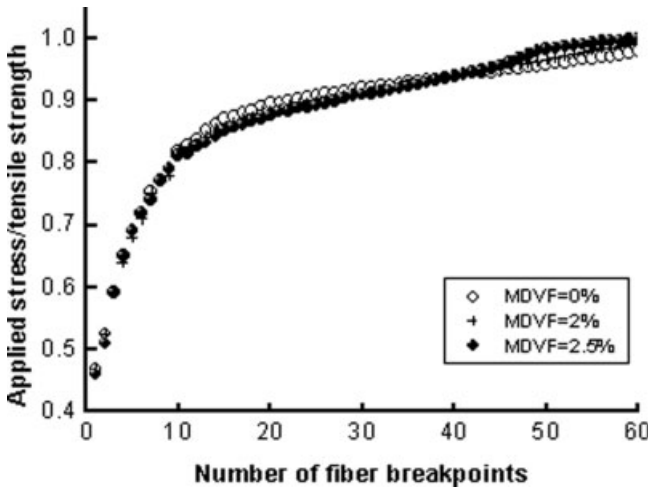

Figure 7 Normalized applied stress versus the number of fiber breakpoints.

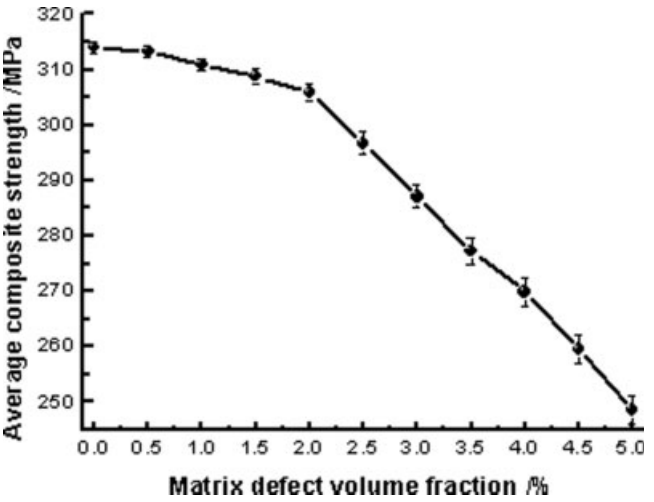

Figure 9 Average composite strength versus MDVF for composites with $m_F = 10$.

loads, the data show a monotonically increasing tendency for the composites having various MDVFs. The normalized strengths and positions (not shown) of the first 40 fiber breakpoints are almost the same for the composites with different MDVFs, but there are some differences in the positions of the 40–60 breakpoints, which lead to some changes in the normalized strengths. When the applied stress reaches the composite strength, the more matrix defects there are in the composite, the fewer fiber breakpoints there are. Figure 8 shows the number of fiber breakpoints versus the strain for composites with and without matrix defects. The first fiber breakpoint occurs at about $\varepsilon = 1.1\%$ for the composites having various MDVFs. Over a range of $\varepsilon = 1.1$–2.6%, the fibers break one by one. In some cases, two or more breakpoints occur in the same fiber. As the extensional strain increases to about 2.6%, no new fiber breakpoints form. The additional strain is accommodated by the further opening of the existing fiber breakpoints or by the fracture propagating into the matrix. That is, the fiber fracture reaches saturation.

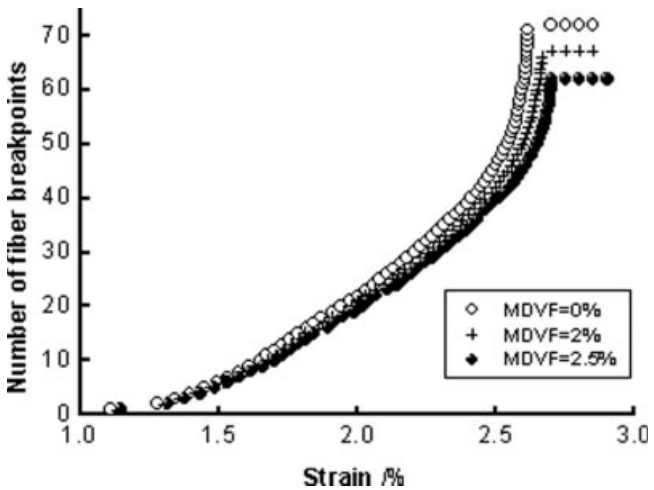

Figure 8 Number of fiber breakpoints versus the strain.

Figure 9 shows the average composite strength as a function of MDVF for composites with $m_F = 10$. The strength of the composite is reduced slowly with an increase in the MDVF when the MDVF is small. There is a quick reduction of the strength of the composite with the increase in the MDVF when the MDVF reaches 2%. Twenty-five Monte Carlo samples with different fiber strengths were simulated for fibers with m_F values of 5 and 10, respectively, for composites with and without matrix defects. $m_F = 5$ indicates that a composite is relatively uniform, and $m_F = 10$ indicates that the composite is relatively uneven. The strength distributions for $m_F = 5$ and $m_F = 10$ are shown in Figure 10, where the strengths are normalized by σ_c and the data are plotted in the Weibull form, $\ln(\sigma/\sigma_c)$ versus $\ln[-\ln(1 - P)]$ (where P is the probability). The composites with matrix defects have lower strengths and broader failure distributions. The rate of the strength decrease with increasing MDVF is larger for composites with smaller m_F. For instance, the strength decrease of the composites with MDVF = 0% and MDVF = 2.5% was about 4% when m_F was 10; this increased to about 5.3% when m_F was 5. In Figure 10, when m_F is 5, the failure strength at $P = 0.3$ $\{\ln[-\ln(1 - P)] = -1.03\}$ decreases by 2.3% at MDVF = 2% and by 4% at MDVF = 2.5%.

CONCLUSIONS

The shape of a small matrix defect has almost no effect on the stress distribution of fiber-reinforced polypropylene-matrix composites, except for the interfacial shear stress distribution. The stress concentrations

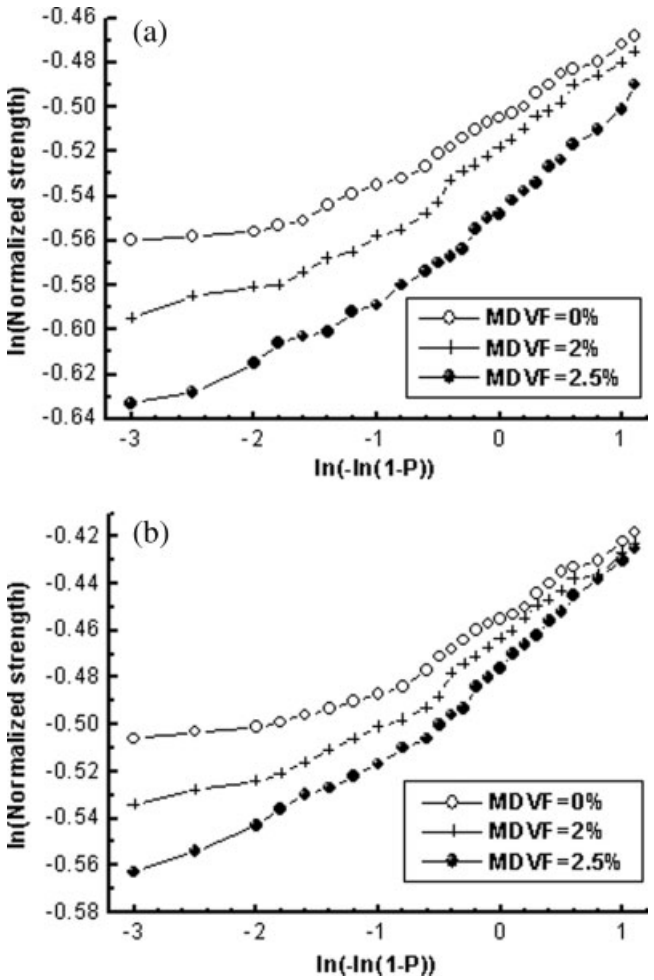

Figure 10 Normalized strength distributions plotted in the Weibull form for composites having various MDVFs: (a) $m_F = 5$ and (b) $m_F = 10$.

resulting from small matrix defects with different sizes on the nearest neighbor fibers are almost the same.

The damage evolution of fiber-reinforced polypropylene-matrix composites with matrix defects has been studied via a Monte Carlo technique combined with the finite element method. With an increase in the MDVF, the rate of the composite strength decrease is larger for composites with smaller m_F.

The strength decrease of composites with small MDVFs can be neglected. This means that it is accurate to use the shear-lag models and Green's function methods to predict the tensile strength of composites even though the axial stresses in the matrix are neglected.

References

1. Cox, H. L. Br J Appl Phys 1952, 3, 72.
2. Hedgepeth, J. M. NASA TND-822; NASA: Washington, DC, 1961.
3. Hedgepeth, J. M.; Van Dyke, P. J Compos Mater 1967, 1, 294.
4. Zeng, Q. D.; Ling, L.; Wang, Z. L. Compos Sci Technol 1996, 56, 1191.
5. Zeng, Q. D.; Wang, Z. L.; Ling, L. J Compos Mater 1997, 57, 129.
6. Beyerlein, I. J.; Phoenix, S. L. J Mech Phys Solids 1996, 44, 1997.
7. Beyerlein, I. J.; Phoenix, S. L. Eng Fract Mech 1997, 57, 241.
8. Zhou, S. J.; Curtin, W. A. Acta Metall Mater 1995, 43, 3093.
9. Ibnabdeljalil, M.; Curtin, W. A. Int J Solids Struct 1997, 34, 2649.
10. Curtin, W. A. Adv Appl Mech 1999, 36, 163.
11. Landis, C. M.; McMeeking, R. M. Int J Solids Struct 1999, 36, 4333.
12. Xia, Z.; Okabe, T.; Curtin, W. A. Compos Sci Technol 2002, 62, 1141.
13. Okabe, T.; Takeda, N. Compos Sci Technol 2001, 61, 1789.
14. Okabe, T.; Takeda, N. Compos A 2002, 33, 1327.
15. Xia, Z.; Curtin, W. A. Compos Sci Technol 2001, 61, 2247.
16. Herakovich, C. T. Inelastic Behaviour of Composite Materials; American Society of Mechanical Engineers: New York, 1975.
17. Brandt, A. M. Cement-Based Composites: Materials, Mechanical Properties and Performance; Chapman & Hall: London, 1995.
18. Jao, S. H.; Frederick, J. M. J Compos Mater 1992, 26, 2632.
19. Curtin, W. A. Compos Sci Technol 2000, 60, 543.
20. Okabe, T.; Takeda, N.; Kamoshida, Y.; Shimizu, M.; Curtin, W. A. Compos Sci Technol 2001, 61, 1773.
21. Xia, Z.; Curtin, W. A.; Okabe, T. Compos Sci Technol 2002, 62, 1279.
22. Zhao, F. M.; Takeda, N. Compos A 2000, 31, 1215.
23. Zhao, F. M.; Okabe, T.; Takeda, N. Compos Sci Technol 2000, 60, 1965.
24. Park, J. M.; Kim, J. W.; Goda, K. Compos Sci Technol 2000, 60, 439.
25. Okabe, T.; Takeda, N. Compos Sci Technol 2002, 62, 2053.
26. Xia, Z.; Okabe, T.; Park, J. M.; Curtin, W. A.; Takeda, N. Compos Sci Technol 2003, 62, 1411.
27. Xia, Z.; Curtin, W. A. Acta Mater 2000, 48, 4879.
28. Xia, Z.; Curtin, W. A. Acta Mater 2001, 49, 1633.
29. Yamada, Y.; Yoshimura, N.; Sakurai, T. Int Mech Sci 1968, 10, 343.
30. Goda, K. Compos Sci Technol 1999, 59, 1871.
31. Goda, K. Int J Plast 2002, 18, 1729.
32. Schmauder, S. Annu Rev Mater Res 2002, 32, 437.